JET–X Info DOC

S. Campana, S. Covino, L. Stella, G. Tagliaferri

This document is still being developed
and should be used with caution

Contents

Abstract

This document describes the main characteristics of the Joint European X–ray Telescope (JET–X) to be flown on the SPECTRUM RÖNTGEN–γ observatory. It is intended to help scientists and/or committees assessing the scientific capabilities of JET–X (also through detailed simulations). This document is available as a compressed postscript file at Brera Observatory WWW JET–X pages (http://jetx.merate.mi.astro.it/jetx.hmtl). A structured HTML document is also accessible.

1 Introduction

The Joint European X–ray Telescope (JET–X) is one of the core scientific instruments of the SPECTRUM RÖNTGEN–γ astrophysics mission. The project is a collaboration of British, Italian and Russian consortia, with the participation of the Max Planck Institut (Germany). JET–X is designed to study the emission from X–ray sources in the band of 0.3–10 keV; in particular to meet primary scientific goals in cosmology and extragalactic astronomy. JET–X consists of two identical, coaligned X–ray telescopes, each with a spatial resolution of better than 20 arcsec Half Energy Width. Focal plane imaging is provided by cooled X–ray sensitive CCD detectors which combine high spatial resolution with good spectral resolution, including coverage of the iron line complex around 7 keV at a resolution of $\Delta E/E \sim 2\%$. Each telescope is composed of a nested array of 12 mirror shells with Wolter I geometry, manufactured by an electroforming replica process. The total (2 telescopes) effective area of the X–ray mirrors is 330 cm^2 at 1.5 keV and 145 cm^2 at 8.1 keV.

The purpose of this document is to give an extensive description of the JET–X characteristics and to provide all information necessary to re-assess in a quantitative fashion the scientific capabilities of JET–X, as the mission approaches fruition. This document is available as a compressed postscript file at Brera Observatory WWW JET–X pages (http://www.merate.mi.astro.it/~xanadu/jetx.hmtl). A structured HTML document is also accessible. Publications related to the project, as well as several tools to aid astronomers to prepare JET–X observing proposals, are on-line at the same WWW site Some of the items above have been prepared in collaboration with the SAX–SDC. **Users should be aware that the current JET–X matrix involves a number of approximations. A more accurate matrix will be available in the second half of 1997 as a results of the the final end-to-end ground calibrations to be carried out at the Panter facility.**

In section II a general description of the SPECTRUM RÖNTGEN–γ (SPECTR–RG) observatory is given, together with a brief survey of the main capabilities of the onboard instruments . A summary of the main scientific objectives of the mission and of time shares is also given. Section III consists of a more extensive description of the JET–X system design. Section IV is devoted to the description of the JET–X mirrors as well as of the latest calibration results. In section V an overview of the CCD detectors is presented together with the filter design. Finally, section VI is intended to provide information for a quantitative assessment of the JET–X scientific capabilities; this includes tools for evaluating source detectability and rates and carrying out detailed numerical simulations and analysis of simulated data.

2 SPECTR–RG Overview

2.1 Introduction

The astrophysical observatory SPECTR–RG is a joint space project of more than twelve countries. SPECTR–RG carries two different instruments based on grazing incidence optics for X–ray astronomy: JET–X (0.3–10 keV) and SODART (0.2–25 keV using different detectors). Beside the X–ray band, the SPECTR–RG response extends toward the far–ultraviolet thanks to the FUVITA (91.2–120 nm) and TAUVEX (140–300 nm) telescopes and toward the hard X–rays thanks to the MART-LIME coded mask telescope (5–150 keV; see figure 1 and table 1).

The main characteristics of SPECTR–RG are large collecting area X–ray mirrors combined with good angular (ranging from ~ 20 arcsec to ~ 3 arcmin) and energy resolution ($\Delta E/E \sim 2 \div 20\%$ at 7 keV, and $0.03 \div 0.1\%$ with the Bragg spectrometer) detectors. This, together with the capability of observing sources over an extremely large energy band, will enable varied and unique scientific programs to be carried out. The other important capability of SPECTR–RG is the ability of continuously monitoring the full sky (except for an area of about 4% of the sky around the sun) in the X–ray energy band 2–25 keV with 6 X–ray pinhole cameras (MOXE). From the existing catalogs, it is estimated that MOXE will monitor ~ 300 sources each day with a flux $> 2\,$mCrab in the 2–10 keV energy band. MOXE will also detect hundreds of gamma–ray bursts and locate them within an $\sim 1^\circ$ error box.

The SPECTR–RG observatory is scheduled for launch in late 1998. A Russian PROTON rocket will take the spacecraft on to a highly eccentric 4 days orbit with inclination 51.6 degrees. Initially, the apogee of the orbit will be 200 000 km, perigee 500 km. Such an orbit will enable to perform virtually uninterrupted X–ray observations during three out of four days, when the spacecraft will be beyond the radiation belts. In two years the orbit perigee will increase to $> 40\,000$ km, and observations will be possible over the entire SPECTR–RG orbit.

Spacecraft operations will be carried out from the Schelkovo tracking station in the Moscow district. Direct contacts between satellite and ground station will be performed once per day for a period of about 4 hours. A low speed telemetry channel (16 kbps) will be used for housekeeping data; science data will be telemetered at 1 Mbps. The expected amount of raw scientific data from SPECTR–RG is ~ 10 Gb per day. The capacity of the on board memory is usually enough to store the data accumulated during 24 hours of observations (depending on the X–ray source count rates). The spacecraft is capable of observing up to 10 different targets per day, the repointings being performed automatically without direct contact with the ground station. The status of the instruments will be monitored by the instrument teams at the Quick Look Facility (QLF) located at Space Research Institute (IKI) in Moscow, where the telemetry will be transmitted from the ground station in near–real time.

	JET–X	SODART
Angular Res.	$<$ 20 arcsec HEW at 8 keV	$\sim$ 3 arcmin
Energy Res.	$\Delta E/E = 2\%$ @ 7 keV	$\Delta E/E = 12\%$ (LEPC and HEPC @ 7 keV), 3% (SIXA @ 6 keV) and 0.03–1.8% (OXS)
Effective Area (Mirrors)	$\sim$ 165 cm^2 at 1.5 keV (1 tel.), $\sim$ 73 cm^2 at 8 keV (1 tel.)	$\sim$ 1460 cm^2 at 2 keV (1 tel.), $\sim$ 1120 cm^2 at 8 keV (1 tel.),
Field of View	27×20 arcmin^2	from 25 to 60 arcmin^2
Energy Range	0.3–10 keV	0.2–8 keV (LEPC), 2–25 keV (HEPC), 0.2–7.4 keV (OXS), 0.5–20 keV (SIXA)
	MART–LIME	**MOXE**
Angular Res.	8.6 arcmin	2.4×9.7 degrees
Resolution	$\Delta E/E = 5\%$	$\Delta E/E = 20\%$ at 6 keV
Effective Area	$\sim$ 1500 cm^2 for $15 < E < 50$ keV, $\sim$ 200 cm^2 E<15 and E>50 keV	$\sim$ 1.4 cm^2 at 6 keV (1 pinhole)
Field of View	6×6 square degree	94×94 square degree
Energy Range	5–150 keV	2–25 keV
	FUVITA	**TAUVEX**
Angular Res.	10 arcsec	6–8 arcsec
Effective Area	0.2 cm^2	
Field of View	1.2 square degree	$\sim$ 0.9 square degree
Energy Range	91.2–120 nm	140–300 nm

Table 1: Summary of SPECTR–RG instrument performances.

2.2 SPECTR–RG Program Overview

The main scientific instruments of the SPECTR–RG are (see also figure 1 and table 1):

1. JET–X, two multimirror grazing incidence X–ray telescopes. Both the two coaligned multimirror systems have cooled CCD as X–ray detectors and will provide high angular resolution imaging ($<$ 20 arcsec HEW at 8 keV) and fine spectroscopy ($\Delta E/E = 2\%$ at 7 keV). The effective area of each mirror module is of $\sim 165\,\mathrm{cm}^2$ at 1.5 keV and $\sim 73\,\mathrm{cm}^2$ at 8 keV. The total effective area (mirror+filter+CCDs) of one module is of 100 cm^s and 16 cm^2 at 1.5 keV and 8.1 keV, respectively (for single pixel events, see below). The field of view is 27×20 arcmin^2.

2. SODART, two multimirror grazing incidence X–ray telescopes. Different focal plane detectors are present: the Low Energy Proportional Counter (LEPC, 0.2–8 keV) and High Energy Proportional Counter (HEPC, 2–25 keV), the Solid State Spectrometer Array (SIXA, 0.5–20 keV), the Objective Crystal Spectrometer (OXS, 5 energy bands depending on the chosen crystal covering 0.15–7.4 keV) and the Complex of focal X–ray detectors (KFRD) consisting of two indipendent position sensitive spectrometers (2–25 keV), as well as the Stellar X–ray Polarimeter (SXRP) consisting of a Bragg reflection based and a Thomson scattering based instruments. The angular resolution of imaging is dominated by the mirror shells and is $\lesssim 3$ arcmin. The energy resolution is 12% at 7 keV for LEPC and HEPC

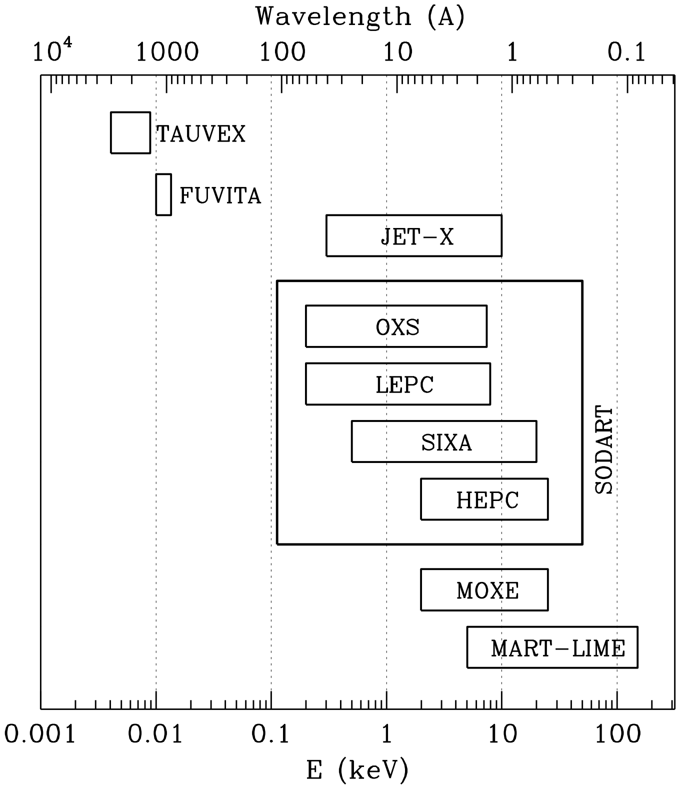

Figure 1: Energy range covered by SPECTR–RG instruments.

($\Delta E/E \simeq 0.32 \times \sqrt{E(keV)}^{-1}$), 3% for SIXA and 0.03–1.8% OXS. Each mirror module has an effective area of $\sim 1460\,\mathrm{cm}^2$ at 2 keV, $\sim 1100\ \mathrm{cm}^2$ at 8 keV and $\sim 94\,\mathrm{cm}^2$ at 20 keV, resulting in total effective areas of ~ 1000 cm^2 at 2 keV for LEPC (one mirror module), 750 cm^2 at 8 keV for HEPC (one mirror module) and $\sim 1050\ \mathrm{cm}^2$ at 8 keV and $\sim 80\ \mathrm{cm}^2$ at 20 keV for SIXA. The field of view of the different focal plane detectors ranges between 25 and 60 arcmin.

3. MART-LIME, the base-line photon detection system of MART-LIME is a high pressure (5 bar) Xenon-filled Multi Wire Proportional Counter (MWPC) behind a coded mask aperture. The MWPC will be sensitive to energies in the hard X–ray range 5–150 keV with an efficiency higher than 10%. The MWPC field of view is 6×6 square degree; the angular resolution is 8.6 arcmin, while the effective area is $\sim 1500\,\mathrm{cm}^2$ for $15 < E < 50$ keV and $\sim 200\,\mathrm{cm}^2$ for $E < 15$ and $E > 50$ keV.

4. TAUVEX, three coaligned ultraviolet telescopes that will image the same 0.9 degree field from 140 to 300 nm, using different filters. TAUVEX will

be able to detect point sources with a monocromatic UV magnitude of 19 in three broad-band-filter in 4 hour.

5. FUVITA consists of two normal incidence telescopes for far ultraviolet in the energy range between 91.2 nm and 120 nm. FUVITA, with an effective area of 0.2 cm^2, will image the sky at a 10 arcsec level over a 1.2 degree field of view with a limiting sensitivity of 10^{-5} photons s^{-1} cm^{-2} $Å^{-1}$ (for point sources with 1 day observing time).

6. MOXE consists of an array of 6 X–ray pinhole cameras (one face of a cube), sensitive from 2 to 25 keV, which views the whole sky, except for a 20×80 degree patch which includes the Sun. The sensitivity will be of ~ 4 mCrab in 4 hours or 2 mCrab in 24 hours. Every 10 mCrab source can be monitored on time scale of an hour and bright sources (> 100 mCrab) on time scale of minutes. The confusion limit for MOXE is estimated to be at ~ 1 mCrab (with higher values toward the galactic center and other crowded regions). The on-axis angular resolution is of 2.4×9.7 square degree. For a given source, the orientation of the long axis of the aperture as projected on the sky will vary from one pointing of SPECTR–RG to the next. Two sources which are confused in one pointing may not be confused when the projected aperture is turned to a different angle. So it is expected that over different pointings the angular resolution will be of 2.4 degree in both directions (i.e. 2.4×2.4 square degree).

All these instruments, except MOXE which is mounted on the scientific platform, have optical axes coaligned.

The SPECTR–RG automatic space vehicle incorporate:

2.3 Launch Vehicle

- Proton–2 launcher
- booster
- spacecraft SPECTR–RG (figure 2)

Launcher and booster mass of 700 000 kg.

- Spacecraft 6 000 kg
  - astrophysical module 2 570 (+235) kg
  - platform with scientific equipment 415 (+35) kg
  - scientific equipment complement 2 500 (+250) kg

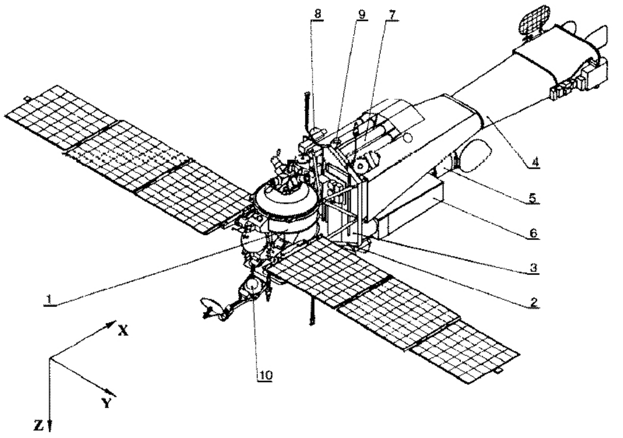

1. Astrophysical module
2. Adapter truss structure
3. Scientific equipment platform
4. SODART X-ray telescope
5. JET-X X-ray telescope
6. MART X-ray telescope
7. EUVITA UV telescope
8. MOXE X-ray survey monitor
9. SPIN gamma burst spektrometer
10. DIOGEN gamma burst spektrometer

Figure 2: The SPECTR–RG spacecraft

2.4 Pointing Performances

SPECTR–RG will have a pointing accuracy of:
– with Star Tracker < 3.5 arcmin;
– with Sun and Star Sensor < 4.5 arcmin;
– stabilization accuracy < 2.5 arcmin.

After calibration of misalignment, the pointing accuracy is of:
– with Star Tracker < 2 arcmin;
– with Sun and Star Sensor < 4.5 arcmin.

The pointing stability should be better than 5 arcsec over a 1 minute period with a limit cycle of 30 arcsec from the demanded attitude.

Moreover, JET–X is equipped with an additional attitude monitor which will allow a post-facto attitude reconstruction better than 30 arcsec (see below).

2.5 Scientific Objectives

The primary instruments of SPECTR–RG are the high performance multimirror X–ray telescopes JET–X and SODART, the coded mask MART-LIME and the All-Sky monitor MOXE. They will enable:

- To study the cooling flows and the distribution of the intergalactic gas and heavy elements in the clusters of galaxies. To study cluster substructures and temperature maps. To study the hidden mass in clusters of galaxies. To determine the Hubble constant through the Sunyaev–Zeldovich effect.

- To search and study high redshift quasars. To perform deep surveys and source counts.

- To study AGNs determining spectral shape and dynamics of the variable continuum on a very large energy band and high sensitivity. To determine the variability between the continuum and narrow spectral feature ratios. To do fine spectroscopy and polarimetry of individual objects, spectra of high redshift objects up to 20 keV.

- To study black hole and neutron star binary systems, determining the shape and variability of the continuum and narrow spectral features as a function of orbital and rotational phases. To study ultra–soft sources. To do fine spectroscopy and polarimetry of individual objects. To perform all sky monitoring and search for transient sources. To do long term monitoring of bright Galactic X–ray sources, including timing of bright pulsars. To study supernova remnants through spatially resolved high resolution spectra. To monitor the central part of the Galaxy and study both diffuse and point sources.

- To measure the elemental abundances and Emission–Measure distribution both for single field stars and for stars in open clusters. This will allow to distinguish between truly evolutionary effects on stellar activity and effects primarily due to the star rotation rate. It will also be possible to study without interruption the rotational modulation and occultation of the coronal emission in short period eclipsing binary systems (for the first time after EXOSAT).

- To study γ–ray bursts, with their coarse localization and subsequent fine spectroscopy. To serendipitously detect γ–ray bursts within field of view of imaging instruments (MART-LIME, SODART).

2.6 Observation Scheduling

The observing time of each pointed instrument is divided in primary and secondary time. Each instrument will select the targets during its primary time and this will be assigned to each instrument on a one orbit basis. During secondary time it will observe the targets selected by the prime–time instrument for that observations. All pointing instruments are coaligned except when the Bragg spectrometer, which points at 90°, is in use in front of the SODART telescope. The allocation of prime time is as follow:

- SODART 45%
- JET–X 35%
- MART-LIME 10%
- FUVITA 10%

From the point of view of data ownership, both the primary and secondary observing time of each instrument is divided between participating countries according to data share agreements, based on their involvement in the design and manufacturing of the instruments. The 55% of observing time of each instrument belongs to Russia as a return for the design of the spacecraft, the launch and the operations of the observatory. For JET–X the remaining 45% of observing time is assigned as follows: 19.5% United Kingdom, 18.5% Italy, 6% Germany and 1% Russia. Assuming an efficiency of 72%, this should correspond to 1470 and 2730 ks/yr of Italian primary and secondary time, respectively. However, about 20% of the Italian time must be assigned to proposals with at least one German Co-I.

2.7 Time Allocation Procedure

The mission observations planning cycle will be one year. The allocation of time, both primary and secondary, shall be in accord with the fraction agreed by instrument and nationality. A major aim of the time allocation shall be the maximisation of the scientific return from the SPECTR–RG mission. The scientific data rights will belong to the allocated observer for about one year following the delivery of the data together with a suitable calibration. After the expiration of that period, the data will be open to public access.

There will be 4 types of observations:

- Standard, this is the normal mode of operation for the satellite;
- Time-Critical, a maximum of 5% (**TBC**) of time shall be awarded for observations which require a specific observation period;
- Instrument Target of Opportunity (IToO), a maximum of 5% (**TBC**) shall be awarded by national committees for this type of observations (i.e. cases such as recurrent transients, CV outbursts, etc.) which are expected to occur but whose timing cannot be predicted.
- Observatory target of opportunity (OToO), this category is reserved for event which cannot reasonably be predicted (e.g. a galactic supernova). Up to 2% **TBC** of the observatory time shall be available for such observations.

The selection of proposals, based on scientific merits, will be performed on three levels:

- Selection by national time allocation committees (N–TAC);
- Selection by instrument level time allocation committees (I–TAC);
- Selection by the SPECTR–RG level committee (S–TAC).

At the national level (N–TAC), locally defined rules will be used to provide a target list with supporting scientific cases for each observation. Each nation should plan to propose more observations than its data share would suggest to allow for the removal of duplicated or impossible requests. At the instrument level (I–TAC) each major instrument will compile an optimised observing schedule for its allocated prime time and provide details of this to the final level where the S–TAC will produce the final list of primary targets for SPECTR–RG.

3 JET–X Overview

The Joint European Telescope for X–rays (JET–X) is a collaborative project developed by a consortium of scientific institutes in the United Kingdom, Italy, Germany and Russia. The JET–X telescope is one of the key instruments onboard the SPECTR–RG satellite.

3.1 System Design

The two identical, coaligned, imaging telescopes of JET–X consist of a nested array of 12 mirror shells with a focal length of 3.5 m and a diameter of 0.3 m. Focal plane imaging is provided by passively cooled CCD detectors. The combined response of the CCD and the X–ray mirror covers a bandpass from 0.3 to 10 keV.

Spacecraft drift and thermal distortion over long observations would lead to image blurring and loss of sensitivity. In particular an expected stability of about 30 arcsec is expected for about 30 hr of observations. JET–X has an attitude monitor that measures the instrument pointing direction, at 1 s intervals, and thereby allowing to correct for drift in pointing between successive CCD frame images (integration time 2.5 s) in the data analysis. The attitude monitor detects and monitors positions of up to four stars in its $4^\circ \times 5.5^\circ$ field of view, allowing for a post facto attitude reconstruction for the JET–X images better than 5 arcsec, through data processing on the ground.

3.2 Requirements on Operations

JET–X operates as a standalone instrument with simple interfaces to the spacecraft. A silicon radiation monitor detector measures the ambient cosmic particle radiation levels, so that the X–ray telescopes can be switched off during solar flares and passages through the Earth's radiation belts. It will normally be observing except during radiation belt passages, part of the ground contacts and when the satellite is in solar eclipse (which will only occur once or twice per year). JET–X operations will continue in parallel to any other prime instrument.

JET–X stores its science data internally in a solid state mass memory which has a capacity of up to 60 Mbytes. This mass memory will be dumped at every ground contact and will require 650 s of dump time assuming the memory is full. Slow housekeeping data will be provided to the spacecraft at the rate of 120 bytes every 60 s during normal operations out of ground contact. During ground contact the housekeeping data rate will increase to 120 bytes every 4 s.

3.3 Sub–systems

The JET–X structure is constructed from three carbon fiber tubular sections. The structure contains the instruments and acts as an optical bench, with which

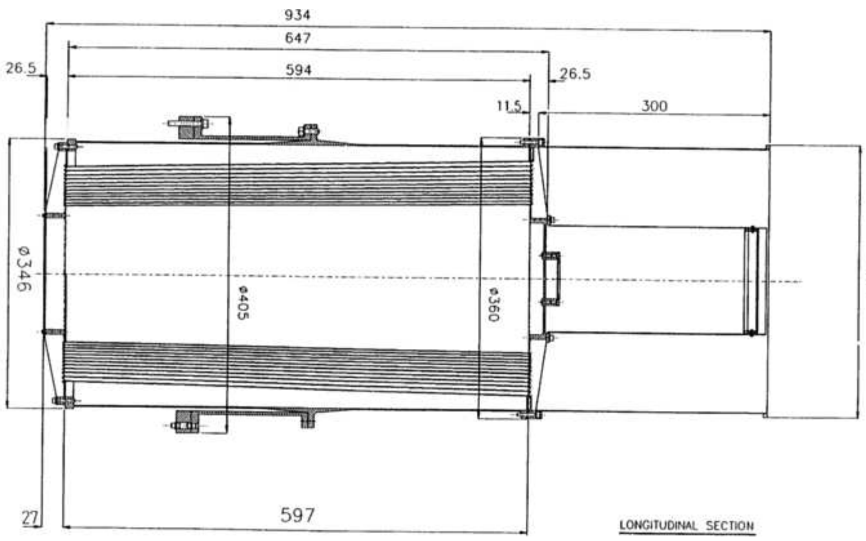

Figure 3: Assembly drawing of the JET–X X–ray optics.

to maintain focus and stable alignment of the X–ray mirrors relative to the focal plane detectors and accurate co–alignment between the X–ray telescopes and the attitude monitor. The forward section of the structure has a deployable door, which remains closed until the satellite has reached its orbit. The function of the door is to protect sensitive optical surfaces from contamination and moisture for ground operations and during launch.

The X–ray mirrors are mounted on a bulkhead in the forward section of the structure. The CCD detectors, together with a shutter and a filter wheel mechanism, are mounted on the focal plane bulkhead, which is part of the rear section of the structure. Each CCD is cooled by a passive radiator which is mounted on the outside of the structure and connected to the CCD cryostat by a thermal link.

The mass of JET–X is 545 kg and the operational power consumption is $\sim 260\,\mathrm{W}$, approximately half of which is used for thermal control.

4 JET–X Mirrors

JET–X consists of two identical and coaligned Wolter I X–ray telescopes each made of 12 nested and confocal mirror shells (see layout in figure 3). These shells are 600 mm long and have diameters ranging from 191 to 300 mm, with a focal length of 3500 mm (see Figure 4). The mirror shells were produced by a replication technique utilising the process which has also been used for the SAX telescopes. An aluminum mandrel is coated with a thin layer of nickel and then superpolished to a surface roughness of ~ 5 Å rms. A layer of gold is then evaporated on the mandrel to provide the mirror reflecting surface. The mandrel is then put in an electrolytic bath where a layer of nickel is deposited. The gold also has a high X–ray reflectivity in the energy range 0.3–10 keV.

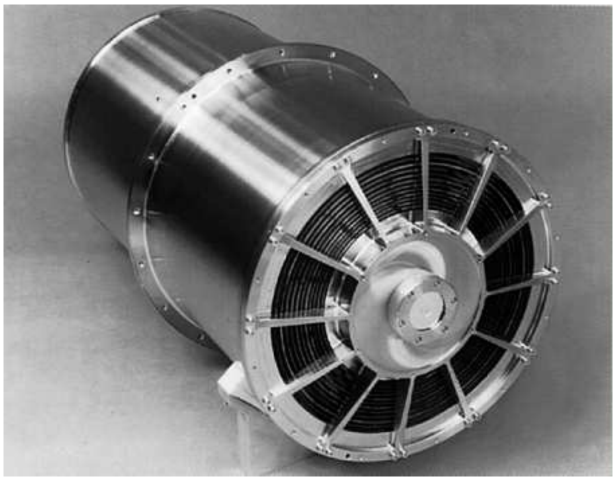

Figure 4: The 12 mirror shells and the mechanical structure are assembled in the the JET–X Flight Model 2.

4.1 Mirror Effective Area and Surface Roughness

The geometric collecting area of each FM is 231.1 cm^2. The JET–X Flight Models were tested at the Panter X–ray testing Facility of the Max Planck Institute, München. The divergence of the Panter Facility X–ray beam causes a loss of area because of the lack of secondary reflection for some photons. This loss amounts to 5%. The twelve arms spider causes a decrease of the useful area of 10%, so that the utilised geometrical area of JET–X FM units at PANTER is 196.7 cm^2.

In order to recover the correct effective area (i.e. for a point source at infinity) we simulated, by means of a ray-tracing software, both a parallel beam (source

Energy (keV)	FM1 cm^2	FM2 cm^2	FM3 cm^2	Theory† cm^2
1.49	158.9±1.1	161.0±0.8	162.5±1.1	164.6
8.05	69.2±0.6	69.5±0.6	62.1±0.4	72.9

Table 2: Mirror effective area measurements for FM1, FM2, FM3*.

* The reported values have been measured at the Panter facility (Germany) with the PSPC engineering model as focal plane detector and have been corrected for a source at infinity. The quoted errors derive from counting statistics.
† Theoretical values for the effective area has been derived from the latest Henke reflectivity tables.

at infinity) and a divergent beam (i.e. Panter source) cases for several energies, deriving the corresponding theoretical effective areas, A_∞ and A_{Panter}. We then normalized the measured effective areas at Panter with the ratio between A_∞ and A_{Panter}. In table 2 we report the measured, on-axis effective area at infinity measured so far at Panter. Figure 5 also shows the on-axis effective area vs. energy obtained with a ray-tracing simulation together with the values obtained from the measurements.

The effective area of the FM1 and FM2 are –3.5% and –2.2% at 1.5 keV lower than the theoretical value, respectively; at 8.1 keV these are –5.0% and –4.7% lower.

The calibration data from the JET–X flight mirrors indicate that the scattering wings of the Point Spread Function (PSF, see below) have a very low surface brightness even at 8.1 keV. The on-axis collecting area losses at 1.5 keV are expected to be totally dominated by geometrical misalignments etc., while the larger losses at 8.1 keV are introduced by X–ray scattering. By using first order scattering theory in the smooth surface limit we estimate a rms roughness of $\sigma \sim 3.5$ Å (for spatial wavelengths $< 10\mu$m).

4.2 Point Spread Function

The on-axis Point Spread Function (PSF) is currently available only for the three energies at which the telescopes have been so far tested at the Panter facility, namely 0.93 (Cu L_α), 1.49 (Al K_α) and 8.05 (Cu K_α) keV (see table 3).

The Half Energy Width (HEW) is always less than 20 arcsec, while the requirement was of a HEW $\leq$ 30 arcsec at 8 keV. Moreover, the actual values should be even better because the Panter measurements provide an overstimate of the HEWs due to the intrinsic width of the X–ray test beam. The 20 arcsec angular resolution in the focal plane corresponds to a scale of 0.340 mm (HEW)

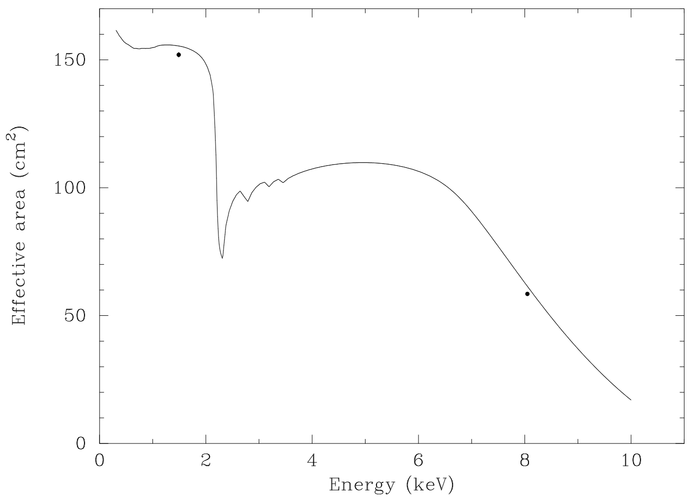

Figure 5: Theoretical mirror effective area curve for a source at 130 m (i.e. the experimental condition at the Panter test facility). The two dots represent the measurements on JET–X FM2 at 1.5 and 8.1 keV.

or to 12.6 CCD pixels.

	ENERGY	FM1	FM2	FM3
HEW (CCD)	0.93 keV	—	12".9	–
90% EEF (PSPC)	0.93 keV	—	37".4	–
HEW (CCD)	1.49 keV	15".1	14".6	16".9
90% EEF (PSPC)	1.49 keV	61".5	46".6	65".0
HEW (CCD)	8.05 keV	18".7	18".8	21".4
90% EEF (PSPC)	8.05 keV	203".5	202".9	192".3

Table 3: Measured HEW and 90% EEF of Jet–X

In order to characterise the on–axis angular resolution of the mirrors, with the CCD in the focal plane, we took an exposure of two sources of same intensity separated by 20 arcsec (by moving the detector by the equivalent of 20 arcsec after half the exposure time). At both 1.5 and 8.1 keV the two sources are well resolved, evidencing the excellent angular resolution of JET–X (see figure 6).

The off–axis PSF, especially at large angles, is dominated by the mirror design and assumes a butterfly shape. Panter tests have shown that for a source at 20 arcmin off-axis the HEW is $\sim$ 65 arcsec at either 1.5 and 8.1 keV (see also section 7.5). This values compares with the 90 arcsec of the ROSAT PSPC.

A large effort has also been devoted to investigate possible contamination from off-axis sources on point sources and from the background on point and extended sources. We first produced an atlas of PSF at different off-axis angles. Indeed we found that photons from sources outside the field of view (FOV) can fall within the CCD due to single reflections (hyperboloid or paraboloid) or directly without hitting the mirrors. Based on recent calibration results and using our ray-tracing simulator, we evaluated the influence of out of FOV sources in terms of CCD contamination. Using astronomical databases we computed the contamination of X–ray bright sources (HEAO A-1) on ROSAT all sky survey (RASS) sources and found that only a very small fraction (0.6%) of RASS sources are contaminated at a level $\gtrsim 5\%$ by bright sources outside the FOV. Spurious (i.e. single or direct) reflections also affect background photons producing an increase in the local background on the detector. We evaluated the impact of this enhanced background on both point and extended sources by means of multi-energy ray-tracing simulations. We concluded that for JET–X this enhanced background has very small effects on source spectra, with respect to the nominal background. As a final step we considered the case of an extended source larger than the CCD field of view, so that autocontamination arises. Also in this case the changes in the spectra due to these spurious reflections are minor.

4.3 Atlas of Point Spread Functions at Different Off-Axis Angles. TBD

TBD

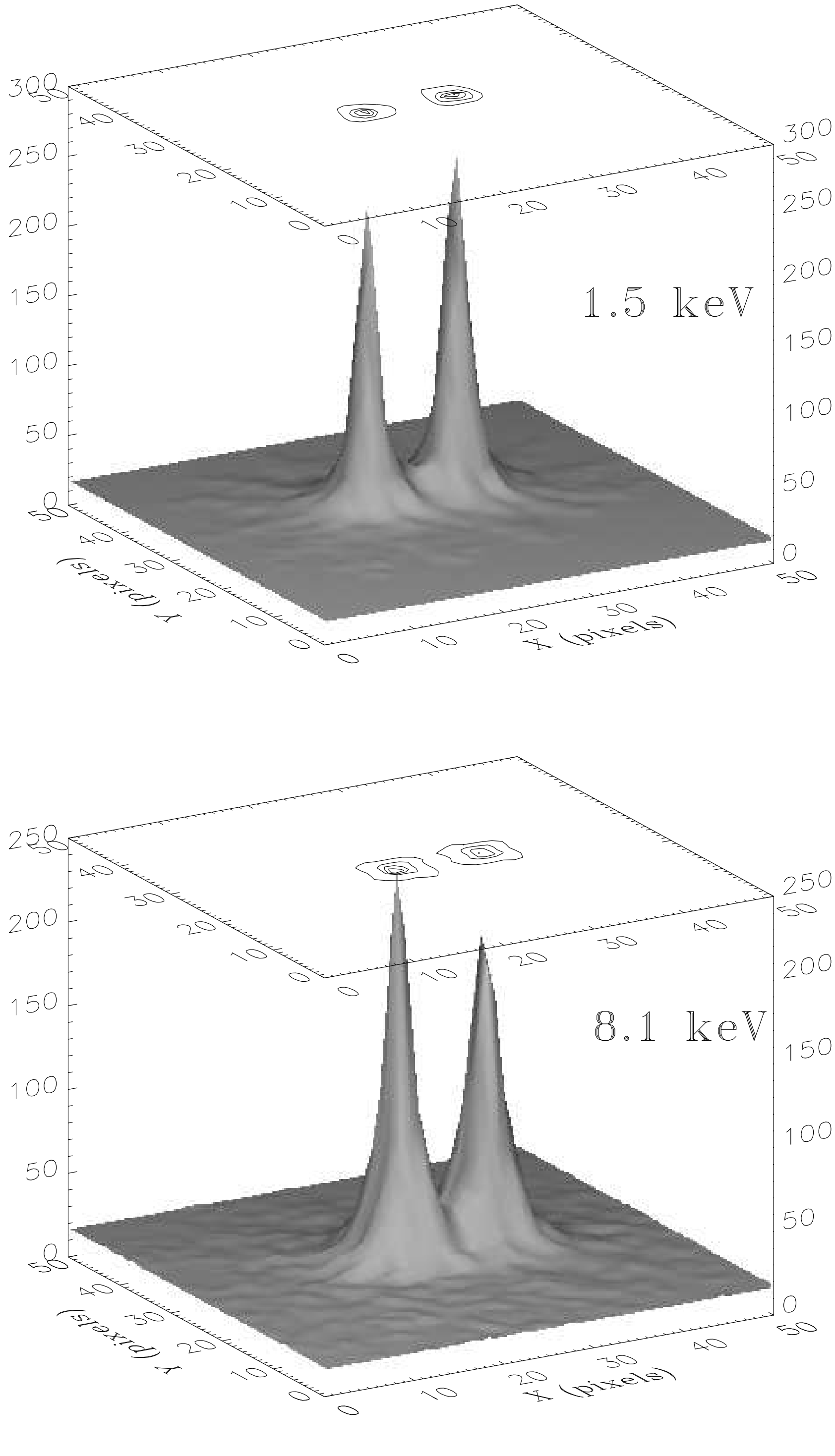

Figure 6: JET–X FM2 CCD images of two sources separated by 20 arcsec at 1.5 keV (upper figure) and 8.1 keV (lower figure).

5 JET–X CCD Detectors

The JET–X CCD cameras are large area (20.7 mm×27.6 mm), multi-pixel (768×1024) devices (see table 4). CCDs have been designed with a wide band (0.3–10 keV) energy response to increase the low energy efficiency: a detection efficiency as high as 90% at 1.5 keV is achieved. The CCD need to be cooled to –80 °C in order to suppress the thermal dark current component of the noise signal and resulting in a readout noise of about 4 electrons for each frame (rms). This low temperature is achieved by passive cooling to deep space through a radiator mounted on the outer structure of JET–X and connected to the focal plane CCD by a rigid thermal link. The thermal link and the CCD are supported from thermally isolating struts inside a cryostat enclosure to locate the CCD at the focus of the X–ray telescope. The cryostat also provide passive shielding and attenuation of the radiation flux encountered by JET–X in orbit. This cryostat structure, which provide a passive shield for the in-orbit radiation flux, mounts a filter drive, with selectable filters to block unwanted optical light, and a radioactive calibration source.

CCD Parameter	Value
Pixel format on chip	1024×768
Image format per pixel (pixels)	512×768
Pixel size	27×27 microns^2
	1.65×1.65 arcsec^2
Field of view	27×20 arcmin^2
Total active depth (epi–layer)	65 microns
Depletion depth	38 microns
Output node gain	~ 4 mV/electron
Readout noise	< 4 electrons rms
Readout rate per pixel	12 microseconds
Dark current at –80 °C	0.004/pixel/s
Image frame time	2.5 s
Operating Temperature (start–of–life)	$180 - 190$ °K
Serial Charge Transfer Inefficiency	$< 1 \times 10^{-5}$ per pixel
Parallel Charge Transfer Inefficiency	$< 1 \times 10^{-5}$ per pixel

Table 4: Characteristics of the JET–X CCDs

5.1 The Focal Plane and CCD layouts

The size of the imaging area in each CCD is 768 pixels (clocking direction) by 512 pixels (frame transfer direction) and an equally sized frame transfer area.

The frame transfer area is shielded from exposure to the sky and acts as a double buffer in order to minimise the dead time of the imaging area during readout. Figure 7 shows the layout as seen from infront of the CCDs, with the frame transfer areas shown hatched. The boresight for each X–Ray Telescope (XRT) is shown as a cross and are intended to be coaligned at ground.

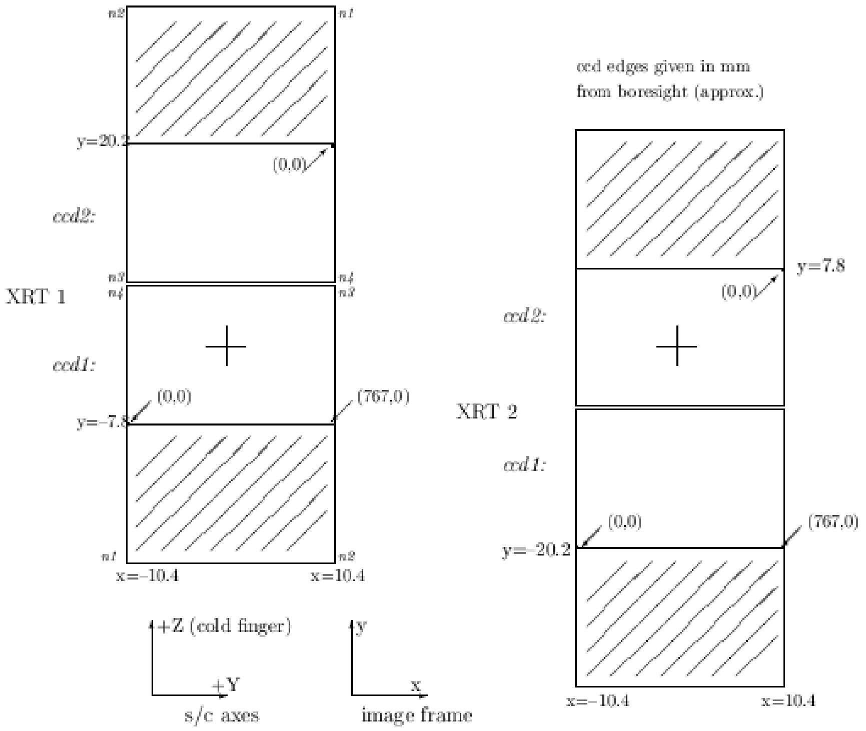

Figure 7: Arrangement of CCDs in Image Plane. The CCDs are viewed from above, to transform these to the sky frame one must view from behind and rotate 180° relative to the spacecraft axes.

From the figure it is also clear that the two telescopes will not see exactly the same part of the sky, only the two on-axis CCDs with the cross will see the same part of the sky, while the other two will see different parts. This different alignment of the two telescope axes has been foreseen to avoid the gap along the junction of the two CCDs. The full 2–CCDs field of view for each telescope will be of $27' \times 20'$ arcmin^2. The field covered by the two telescopes is about $40' \times 20'$ arcmin^2 while the common area of about $13.5' \times 20'$ arcmin^2.

5.2 CCD Linearity and Gain

The CCD linearity was determined (to better than 0.02%) from residuals of a best fit linear regression to the measured center line energies ranging from 523 to 8040 eV, with no systematic trends.

An accurate measurement of the gain has been obtained at the Panter facility at energies ranging from 0.3 to 9.8 keV. The fitted gain has a gradient of 3.715 eV and a zero offset of 0.12 channels. The residuals are less than 7 eV mainly due to blend of the selected lines with nearby ones; flight devices should be calibrated with an accuracy of $\lesssim 4$ eV. The evolution of the gain with time will be monitored through the ^{55}Fe onboard X–ray source.

5.3 Quantum Efficiency

The CCD quantum efficiencies for various classes of events (single pixel, single + double pixels, etc. see below) have been determined at a variety of energies. The quantum efficiency curve have been built up from the Daresbury synchrotron and the Panter test facilities as well as simulations. A particular care was deserved to study the X–ray Absorption Fine Structures (XAFS) around the CCD absorption edges of N, O and Si. The characterisation of these structures is important since ASCA measurements have revealed low-level fine structures in target spectra, which cannot be attributed to celestial sources. In figure 8 is shown the quantum efficiencies for both single events and summed events up to 4 pixels. The solid lines represent a Monte Carlo model. The statistic uncertainties in the individual measurements is less than 1% and based on the residuals, we can estimate the systematic uncertainties to be at a level of 3%. Measurements were also performed to assess the spatial variation of the quantum efficiency revealing a rms scatter of 1.5%.

5.4 The Onboard Calibration Source

There is one ^{55}Fe radioactive source associated with each filter wheel in each of the two X–ray telescopes. They will provide three lines at 1.5, 5.9 and 6.4 keV and will be periodically commanded into the field of view. These lines will be used to perform in-orbit checks of the energy scale, quantum efficiency, spectral resolution and measurements of in-orbit radiation damage to the CCDs through charge transfer efficiency measurements.

5.5 Event Selection and Classification

The electronic system scans through each frame of CCD data and selects events for which the total energy deposited is between the lower and upper given thresholds. As pixels are associated into events only single pixel events or those which

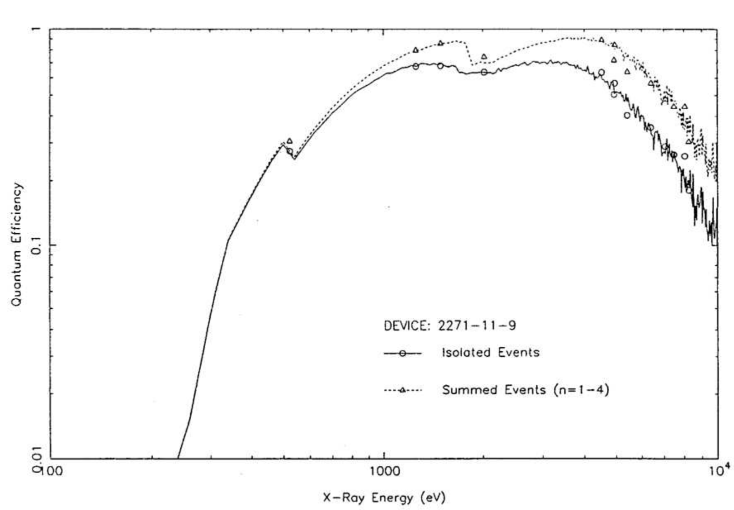

Figure 8: Measured quantum efficiency for a CCD device for single pixel (isolated events) and 1+2+3+4 pixel events. The typical precision of the data points is $\sim 4\%$. The lines show the theoretical response for each of these event types determined from Monte Carlo simulations.

comprise two or more pixels sharing sides are accepted. In timing mode (see below) only adjacency in the row direction is considered. The assigned pixel position for a multiple-pixel event is the location of the first pixel found (i.e. nearest the readout node). The event class is assigned as follows:

- Class 1 - Single pixel events; class 1 events are single pixel events and, because all the charge is limited to one pixel, these give the highest quality energy resolution. Also because background events give rise to predominantly split pixel events, class 1 events give the highest immunity to background contamination. They will be used for detailed spectroscopic studies. For each class 1 event the x and y coordinates plus the pixel energy are stored. Pixels which are corner-to-corner associated are classed as separate, single pixel events.

- Class 2 - Two pixel events; class 2 events are 2 pixel events in which the 2 pixels have side by side adjacency only. For each class 2 event the x and y coordinates of the first pixel plus the total event energy plus the second pixel energy are stored.

- Class 3 - Multiple (greater than 2) pixel events; class 3 events are detected in more than 2 pixels having side to side adjacency. For each class 3 event the x and y coordinates of the first pixel, the total energy and the number of pixel interested are stored.

- Class 4 - Not used in FM.
- Class 5 - Other events; class 5 events are all events for which the summed energy exceeds the maximum energy discriminator. For each class 5 event the x and y coordinates of the first pixel are stored.

5.6 Operating Modes

There are three modes of operation for the CCDs and each CCD mode is independent of the others. Five different JET–X operational modes are foreseen depending on the combination of the basic CCD modes (see table 5). The CCD modes are:

- **Frame Transfer Mode** (standard imaging mode). The primary scientific tasks for the JET–X X–ray telescopes will be to measure the spectra of X–ray images with the focal plane CCDs. For this purpose, the CCDs are used in frame transfer, imaging mode with full spectral resolution. In this mode the image is integrated in the imaging section of the CCD (the areas closest to the optical axis in figure 7) for a period of 2.5 seconds. After this time the image is rapidly transferred (in approximately 6 ms) into the frame store area (shown shaded in figure 7). Then, whilst the image in the store section is read out the next image is integrated in the image section. The time resolution of the frame transfer mode is 2.5 s, which is the time required to read out the image from the store section. The maximum count rate in which the frame transfer mode can operate is determined by the need to avoid coincidence of two events in any pixel during an integration interval (pile-up). Based on present calibration data, the criterion has been adopted that the event rate should be below 0.025 counts/pixel/integration period, which leads to a flux limit of ~ 2 counts/s/point source and corresponds to a source brightness of about ~ 2.5 mCrab.
- **Bright Object Mode.** A Bright Object mode is provided in order to allow imaging of sources with fluxes between one and two orders of magnitude higher than the baseline 2.5 mCrab level. In this mode there are 2 frame transfers during each 2.5 s clock cycle, each of 6 ms duration. During the first phase of the cycle, with duration T_1 seconds, the image is collected, transferred to the frame store region and then discarded. During the second phase, with duration T_2 seconds, the image is collected, transferred to the frame store region and clocked out as normal. The sum of T_1 and T_2 is 2.5 seconds and it is expected that the ratio T_1/T_2 used may be as high as 25, i.e. the real exposure time is not 2.5 s, but a fraction of it, down to a limit 0.1 s every 2.5 s.

- **Timing Mode.** A timing mode is provided for observing bright point sources. One CCD in one telescope is read out continuously at a fast clocking rate. Position information is not preserved but events are time binned to 24 μs resolution at full energy resolution. Only one telescope can be operated in timing mode because of data rate limitations, but the second telescope can continue to operate in frame transfer mode.

		XRT 1		XRT 2	
Operational Mode	Source strength (mCrab)	CCD mode*	Int. time (s/frame)	CCD mode*	Int. time (s/frame)
F1†	< 2.5	FS	2.5	FS	2.5
M1	> 2.5, < 50	BO	see NOTE	FS	2.5
B1	> 50	FS	2.5	FS	2.5
B2	> 50	BO	see NOTE	FS	2.5
B3	> 50	T	n/a	FS	2.5

Table 5: JET–X operational modes.

* FS=Frame Store; BO=Bright Object; T=Timing.
† XRT 1 make no use of the filter (OPEN position).
NOTE: dependent on source. Integration time should scale as source strength: t (seconds)$\sim$ 2.5 / source flux (mCrab).

5.7 The JET–X Filter Design

Thin aluminum filters are commonly used as light blocking filters in X–ray telescope. This is also the case of JET–X, because the CCD focal plane detectors are sensitive to optical light. The current JET–X filter design uses a plastic 2000 Å Lexan substrates to support the aluminum layer. The Lexan is further supported by a 75% transmissive nickel mesh. An aluminum layer thickness of 1100 Å has been chosen from a trade off study between optical leakage and the soft X–ray transmission. The original design had 400 or 800 Å aluminum layers (thin and thick filters respectively), however they suffered of too high optical leakage caused by aluminum oxidation. Furthermore, the aluminum layer is now deposited on a single side only to suppress optical interference effects and to reduce the oxidation levels introduced during the deposition process.

Each telescope has a filter wheel arrangement which can be set during normal operations to one of five positions selectable from the following:

- Two Thick Filters, nominally 2000 Å Lexan, 1100 Å Al;

- Open position;
- Blank position.

The blank position contains a proton shutter and is the default launch position. This position also holds the calibration source for each filter wheel. In the fifth position of the filter wheel a Luxel filter with 2000 Åpolyimide and a yet to be defined layer of aluminum is foreseen.

6 The JET–X data flow. TBD

TBD

7 JET–X Observational Feasibility

7.1 Introduction

This feasibility section is intended to provide a quantitative assessment of the JET–X characteristics and in general of all the information needed to fully address the observability of a source.

Several tools to aid astronomers preparing JET–X observing proposals and providing information about the project have been developed, some of which in collaboration with the SAX–SDC. A response matrix in FITS format can be retrieved from the anonymous account at the Brera Observatory (ftp at antares.merate.mi.astro.it in the directory pub/JETX, retrieve the unitary area response matrix rmf3.fits and the ancillary file arf.fits or the total response matrix rmf2.fits). This will allow, for instance by using the X–ray data analysis package XSPEC, to perform detailed spectral simulations for different X–ray sources. **These matrixes and tools are only valid in first approximation pending to the final end-to-end calibration tests to be carried out at the Panter facility**.

At the address http://www.merate.mi.astro.it/∼xanadu/jetx.hmtl an interactive image simulator, developed by SAX–SDC, is available. This will allow to simulate JET–X observations using the proper PSF, vignetting and effective area characteristics of the instrument. Both random sky and specific part of the sky can be simulated; in the latter case X–ray source fluxes and positions can be taken from the RASS bright source catalog and the WGA catalog (a catalog of sources detected during ROSAT PSPC pointings). HTML tools to compute expected count rates by PIMMS or to determine observing periods by VIEWING can also be found at the same site.

In addition to specific JET–X tools, the on-line Brera High Energy Astrophysics Database Service (HEADS), based on the HEASARC system, can be directly queried. Either through a standard login (**telnet antares.merate.mi.astro.it**, user **xray**, no password required), or a specific HTML interface, the HEADS archive offers a wide range of information from the most used astrophysical catalogs (HST, Hipparcos, NGC, etc.) to the high energy space observatories related databases. Some additional tools to perform coordinate conversion, hydrogen column density estimate, etc. can also be found.

Guest investigators will be asked to quantitatively discuss the feasibility of their proposed JET–X observations. This section provides guidelines as to how to proceed for the calculation (to be complemented with the information from the tools above).

7.2 Scientific Objectives

The scientific potential of JET–X derives from its high spatial and good energy resolution and from the advantageous orbit of SPECTR–RG.

The low intrinsic noise of the system allows long, photon limited exposures, yielding a sensitivity limit near $7 \times 10^{-15}\,\mathrm{erg\,s^{-1}\,cm^{-2}}$ (for one telescope and an exposure time of 10^5 s). The two combined JET–X telescopes provide a limit ten times fainter than the Einstein deep Survey limit and similar to the ROSAT Deep Survey limit. At this sensitivity JET–X will remain un–confused (at 40 beams per source) thanks to an angular resolution better than 20 arcsec HEW at all energies. Also the higher energy response makes JET–X a valuable extension to ROSAT, for example in determining temperature structures in clusters of galaxies, detecting the important Fe K–features in active galaxies, determining temperature and Emission Measure distribution for coeval stars in crowded open cluster, etc.

The major scientific goal of JET–X is a study of faint and/or extended and/or crowded field X–ray sources, by spectroscopy, imaging and timing (while bright, isolated X–ray sources are better studied by SODART). The high resolution optics, low noise detectors and 4–day orbit, combine to emphasise the value of long exposures for JET–X.

The key scientific objectives of JET–X are:

- Deep Fields. Direct measurement of source counts, to a level corresponding to ~ 0.5 of the X–ray background flux (XRB), hence identifying the major constituent(s) of the XRB in the 2–10 keV band.

- Medium Surveys. Broad–band spectroscopy of many X–ray sources detected in the ROSAT survey, yielding information on the possible evolution of the X–ray emission and absorption in AGN, etc.

- Extended Source Spectra. Imaging and spectroscopy of rich clusters of galaxies (and substructures), elliptical galaxies, star open clusters and SNRs to determine their temperature, density and chemical abundance distributions; hence their mass and evolution.

- Single Source Observations. To study, in particular, the variability in flux and spectrum and hence the geometry of individual emission and absorption features (but see also SODART).

In table 6 we summarize the main characteristics of present and future X–ray missions in order to evaluate the JET–X performances and its key capabilities.

7.3 Effective Area

The JET–X effective area will result from the folding of the mirror (see section 4.1), CCD quantum efficiency (see section 5.3) and filter (see section 5.7)

Instrument	Energy range (keV)	Half Energy Width	Effective Area (cm^2)	Energy Resolution ($\Delta E/E$)
ROSAT				
PSPC	0.1–2.4	$\sim 25''$	220 @ 1.5 keV	43% @ 0.9 keV
HRI	0.1–2.4	$\sim 1.7''$	95 @ 1.2 keV	
ASCA				
GIS	0.7–10	$\sim 3'$	300 @ 2 keV (2 T)	7% @ 7 keV
SIS	0.5–10	$\sim 3'$	280 @ 2 keV (2 T†)	2% @ 7 keV
SAX				
LECS	0.1–10	$\sim 3.5'$	56 @ 2 keV	8% @ 6 keV
MECS	1.3–10	$\sim 1.2'$	150 @ 6 keV (3 T)	8% @ 6 keV
PDS	15–300	collimator	500 @ 60 keV	15% @ 60 keV
HPGSPC	4–120	collimator	240 @ 60 keV	4% @ 60 keV
XTE				
PCA	2–60	collimator	7000 @ 10 keV (5 T)	18% @ 6 keV
HEXTE	15–250	collimator	700 @ 30 keV (2 T)	15% @ 60 keV
JET–X	0.3–10	$\lesssim 20''$	200 @ 1.5 keV (2 T*)	2% @ 7 keV
SODART				
LEPC	0.2–8	$\lesssim 3'$	2200 @ 2 keV (2 T)	13% @ 6 keV
HEPC	2–25	$\lesssim 3'$	1800 @ 8 keV (2 T)	13% @ 6 keV
SIXA	0.5–20	$\lesssim 3'$	1030 @ 8 keV (1 T)	3% @ 6 keV
MART-LIME	5–150	$\sim 9'$	1500 @ 20 keV	5% $>$ 35 keV
ABRIXAS	0.5–10 keV	$\sim 3''$	50 @ 2 keV	2% @ 6 keV
XMM (EPIC)	0.1–20	$\lesssim 20''$	2450 @ 6 keV (3 T)	2% @ 6 keV
AXAF				
ACIS	0.2–10	$\sim 1''$	650 @ 1 keV‡	2% @ 6 keV
HRC	0.1–10	$\sim 1''$	300 @ 1 keV	
ASTRO-E				
XRS	0.5–10	$\sim 2'$	400 @ 6 keV	$\sim$ 0.2%
XIS	0.4–10	$\sim 2'$	400 @ 6 keV	$\sim$ 1.5%
HXD	10–700		350 @ 50 keV	7% @ 1 MeV
INTEGRAL				
IBIS	15–10000	$\sim 12'$	$\sim$ 3100	7% @ 100 keV
SPI	20–8000	$\sim 2^o$	$\sim$ 500	0.2% @ 1 MeV
JEM-X	3-35	$\sim 3'$	$\sim$ 1000	15% @ 10 keV

Table 6: Current and planned X–ray missions (excluding all sky monitors).

† Effective area for 1CCD mode.
* Effective area for single pixel events.
‡ Effective area for single plus double photon events.

responses. This curve is depicted in figure 9. We point out however that a complete calibration of all the components has not been carried out (e.g. the filters) so that this curve has to be considered as provisional.

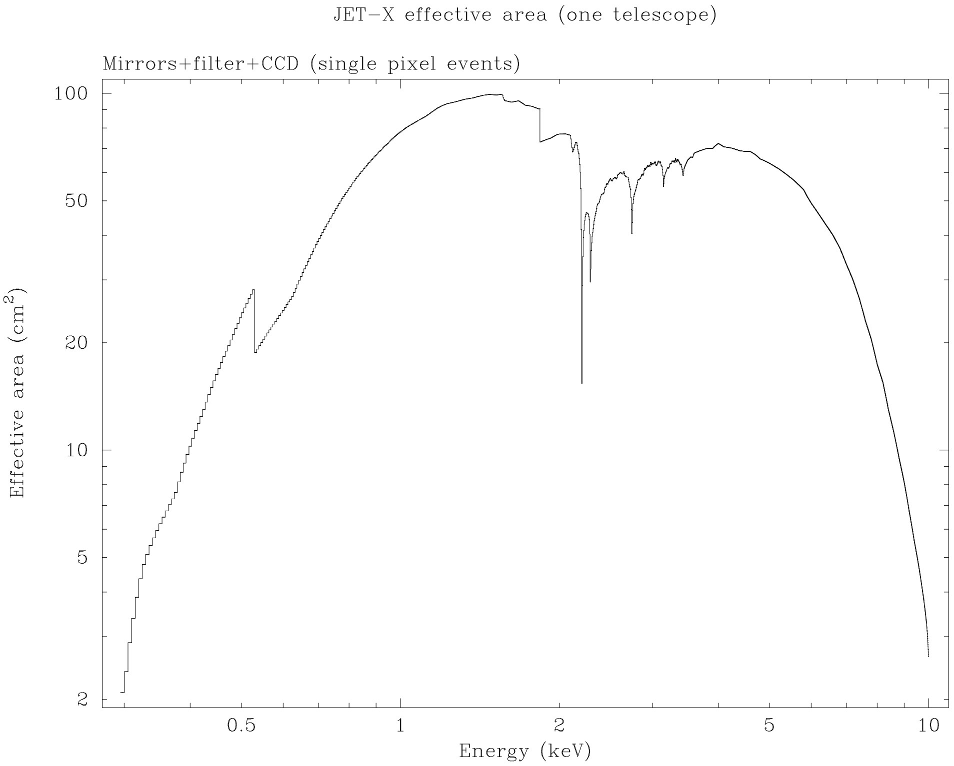

Figure 9: The provisional JET–X effective area folded by the mirror shells, the filter and the CCD responses for one telescope. This area is for one mirror module and ofr single pixel events only. A larger area is achieved by considering all the different event classes (cf. figure 8).

7.4 Energy Resolution

Using different CCD devices produced from flight wafer stock the best-fit to the FWHM energy resolution vs. energy is given by:

$$\Delta E = a_1 \sqrt{1 + a_2\, E}\ \mathrm{eV} \tag{1}$$

where $a_1 = 35.46 \pm 1.3$ eV and $a_2 = (2.0885 \pm 0.2) \times 10^{-3}$ eV^{-1}. As expected, at low energies there is a little difference ($< 0.5\%$) whether one considers single pixel events, or $1 + ... + n$ pixels events. This is because virtually all events are confined to single pixels at these energies. At higher energies, however, ($\gtrsim 5$ keV) there is an increase of about 1% in the width, with each increase in the number of pixels considered to constitute an event. Moreover, it is found that both a_1 and a_2 are (weak) linear functions of the number of pixel events.

7.5 Position Resolution

We consider two source separated when their angular distance is equal or larger than the HEW (see also figure 6). However, the off–axis point response is rather complicate and for large off–axis angles assumes a butterfly shape at all energies, as a consequence of the mirror design. A convenient way to represent this response is by the so-called blur diameter (i.e. the diameter of the circle that contains half of the photons whose center is derived from the Gaussian fit, although the photons are not symmetrically distributed at large off-axis angle). This is shown in figure 10 for energies of 1.5 and 8.1 keV. On–axis the two HEWs are different but at large off–axis angle they become comparable, due to the predominancy of the mirror geometry contribution even at 8.1 keV (instead of the scattering as on-axis).

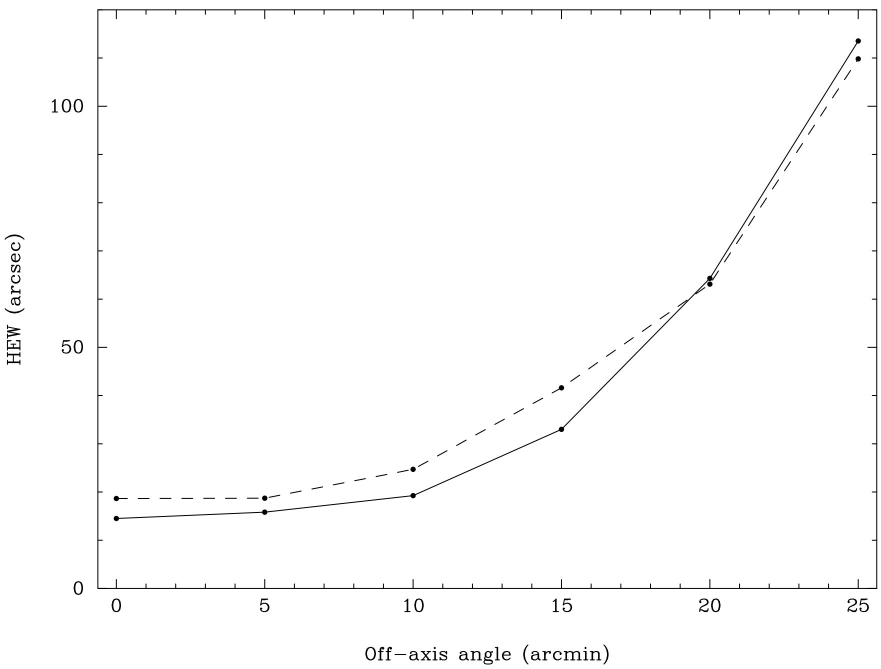

Figure 10: Measured blur diameter as a function of the off-axis angle at 1.5 (continuum line) and 8.1 (dashed line) keV.

7.6 Background

The major component of the JET–X background, before rejection, is the one induced by charged particles. The expected rate is between 2 and 4 particles cm^{-2} s^{-1}, depending on the solar activity. The integral flux above 0.3 keV of the cosmic ray component on the 2 CCD of one mirror module is 13.3 particle s^{-1}. However, the effective cosmic rays rejection of JET–X is very high, resulting in only 0.002 particle s^{-1} on 2 CCDs, with a two pixel cut (see table 7). Thus, the major contribution to the effective (i.e. not rejected) JET–X background comes from the diffuse extragalactic background. The total background component on 2 CCDs is expected to be lower than 0.13 c s^{-1} (for comparison the Crab should have a count rate of about 500 c s^{-1}).

Charged particles (0.3–10 keV; 2 pixel cut)	0.002 c s^{-1}
Diffuse X–ray background: galactic	0.016 c s^{-1}
Diffuse X–ray background: extragalactic	0.057 c s^{-1}
Local production	$<$ 0.057 c s^{-1}
Structure X–rays solar min.	0.001 c s^{-1}
Solar max. + average activity	0.064 c s^{-1}
Cosmic diffuse downscattering	$<$ 0.001 c s^{-1}
TOTAL 0.3–10 keV background	$<$ 0.198 c s^{-1}
TOTAL 0.3–10 keV background estimate	0.13 c s^{-1}

Table 7: JET–X background components for 2 CCDs

7.7 Minimum Detectable Count Rate

The minimum detectable count rate for a given detector depends on the background count rate and on the size of the cell needed to get the source counts for a point source. The minimum detectable count rate as a function of the exposure time can be estimated from the formula:

$$I_{min} = t^{-1/2}\Big(\frac{N_\sigma^2 B_{cell}}{f^2} + \frac{N_{min}^2}{t}\Big)^{1/2} \tag{2}$$

where N_σ is the required significance threshold, B_{cell} is the background count rate in the "detection cell", f is the fraction of the total source count included in the "detection cell", N_{min} is the minimum number of photons required to constitute a detection and t is the integration time.

The JET–X PSF depends on energy (see section 4.2) and hence on the spectrum of the considered source, as well as the position of the source in the field of view. For the calculation shown in figure 11, we assumed a detection circular cell of 30 arcsec radius corresponding to more than 80% of the source photons at 8 keV on axis, a $5\,\sigma$ confidence level of detection and a minimum number of 10 counts per source. For the background we assumed an integral count rate of 0.13 c s^{-1} in the 0.3–10 keV band on the whole detector (2 CCDs $20' \times 27'$). It

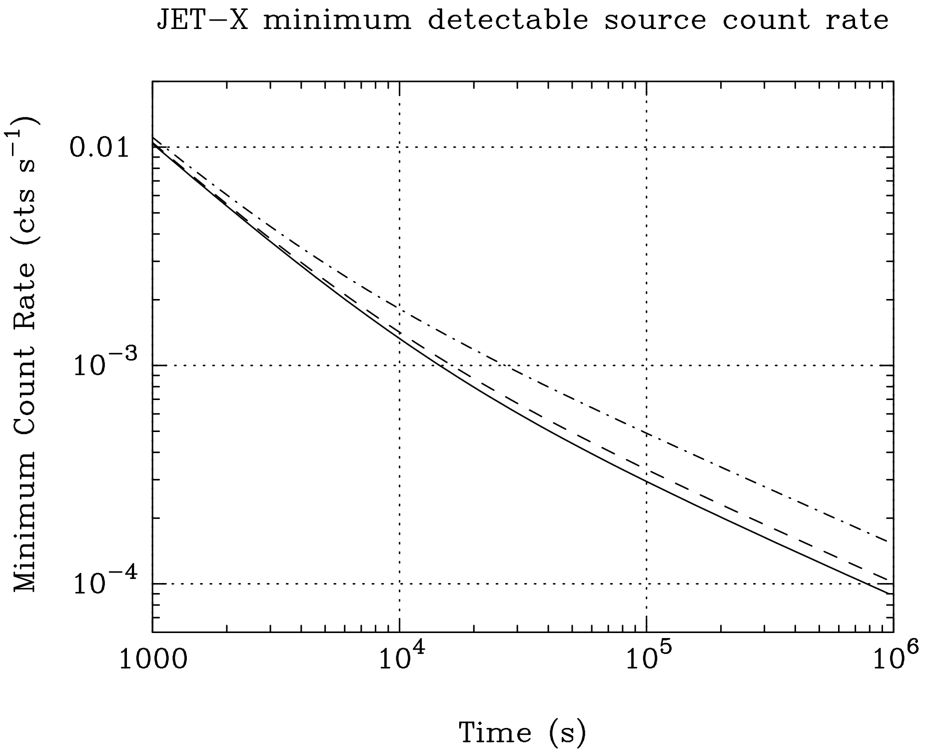

Figure 11: The Minimum JET–X detectable source count rate vs. exposure time. The continuous line corresponds to the nominal expected background (see section 7.6). The dot-dashed line corresponds to a background increased by 30% due to the contribution of spurious reflections. The dashed line corresponds to a background arbitrarily increased by a factor of 3.

is evident from figure 11 that JET–X becomes background-limited for exposure times of $\sim$ 10 ks. For off-axis sources, larger detection cells and consequently larger background values must be used.

7.8 Sensitivity to Line Features and to Source Variability

The JET–X sensitivity to line emission has been calculated for the iron K_α line at 6.4 keV for a range of underlying continuum strengths and for observation durations of 10^4 and 10^5 s (see figure 12). The sensitivity of an instrument to a line feature, I_L, can be expressed as:

$$I_L = \frac{K_\sigma}{A(E)\,F(\Delta E)}\Big(\frac{\Delta E\, I_C(E)\, A(E)\ + B_{cell}}{t}\Big)^{0.5} + \frac{N_{min}}{A(E)\,t} \tag{3}$$

where $A(E)$ is the effective area at energy E, $F(\Delta E)$ is the fraction of line photons falling in the resolution element (taken to be 0.67), I_C is the continuum flux at the line energy in ph cm^{-2} s^{-1} keV^{-1}, B_{cell} is the background flux in c s^{-1} per detection cell, ΔE is the energy resolution at E in keV, K_σ is the significance in the background limited case (taken to be 5) and N_{min} the minimum number of photons required in the photon limited case (taken to be 10).

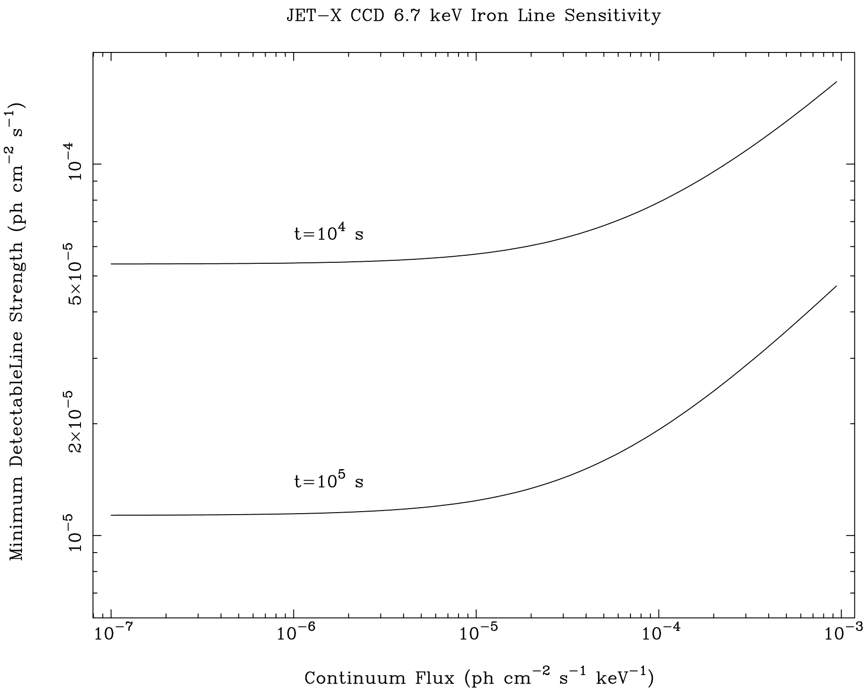

Figure 12: JET–X sensitivity to the 6.7 iron line feature as a function of the underlying continuum for an exposure time of 10^4 s (upper curve) and 10^5 s (lower curve).

The sensitivity of JET–X to source variability is illustrated in figure 13. This shows the time, t, taken to detect a change in the source flux of $X\%$ (i.e. $X = 0.4$ corresponds to a 40% change in the source flux), where S is the source count rate, B the background count rate and K_σ the required significance:

$$t = \frac{K_\sigma^2 \, (S + B + S \times X)}{(S \times Y)^2} \tag{4}$$

Thus for a source and background count rates of 0.1 and 2×10^{-4} c s^{-1}, respectively, $\sim 4\,000$ s are needed to detect a 30% variation in the source flux at $5\,\sigma$ confidence level (see figure 13).

7.9 Expected Count Rates

The expected JET–X count rate depends heavily on the incident source spectrum. It results from the convolution of the source spectrum and the telescope effective

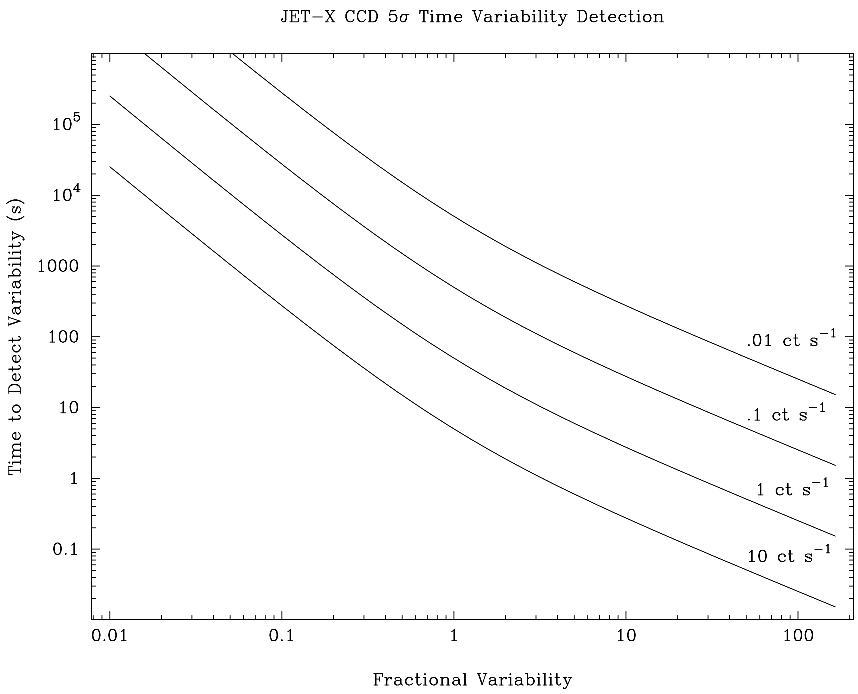

Figure 13: JET–X sensitivity source variability for count rates of 0.01, 0.1, 1 and 10 c s^{-1}.

area, which is a non-trivial function of energy. In order to evaluate the expected count rate, we provide the flux to count rate curves (i.e. the energy conversion factor, ECF) for different values of the interstellar absorption column density, N_H, and for different spectral models:

- power-law with photon index α, see figure 14;
- bremsstrahlung, where KT is the temperature in keV, see figure 15;
- Raymond-Smith, where KT is the temperature in keV: two metallicities have been considered $Z = Z_\odot$ and $Z = 0.3 \times Z_\odot$, see figures 16 and 17;
- black body, where KT is the temperature in keV, see figure 18.

The curves shown in these figures should be used as follows:

- 1) Calculate the expected source flux F_S (in units of 10^{-11} erg s^{-1} cm^{-2} in the JET–X pass band 0.3–10 keV assuming NO interstellar absorption (i.e. the unabsorbed flux);
- 2) Determine the expected interstellar column density;

- 3) Select a spectral model and with the given value of N_H read in the figures the energy conversion factor, ECF;
- 4) Multiply F_S by ECF to obtain the expected JET–X count rate for ONE telescope.

Example:

An Active Galactic Nucleus is characterized by a power-law spectrum with photon index 1.7 and an unabsorbed flux of 7.2×10^{-11} erg s^{-1} cm^{-2} (0.3–10 keV). The interstellar column density in its direction is $N_H = 3 \times 10^{20}$ cm^{-2}. From Figure 14, one obtains a Conversion Factor of ~ 0.18, so that the expected count rate is $0.18 \times 7.2 = 1.3$ c s^{-1} for one telescope.

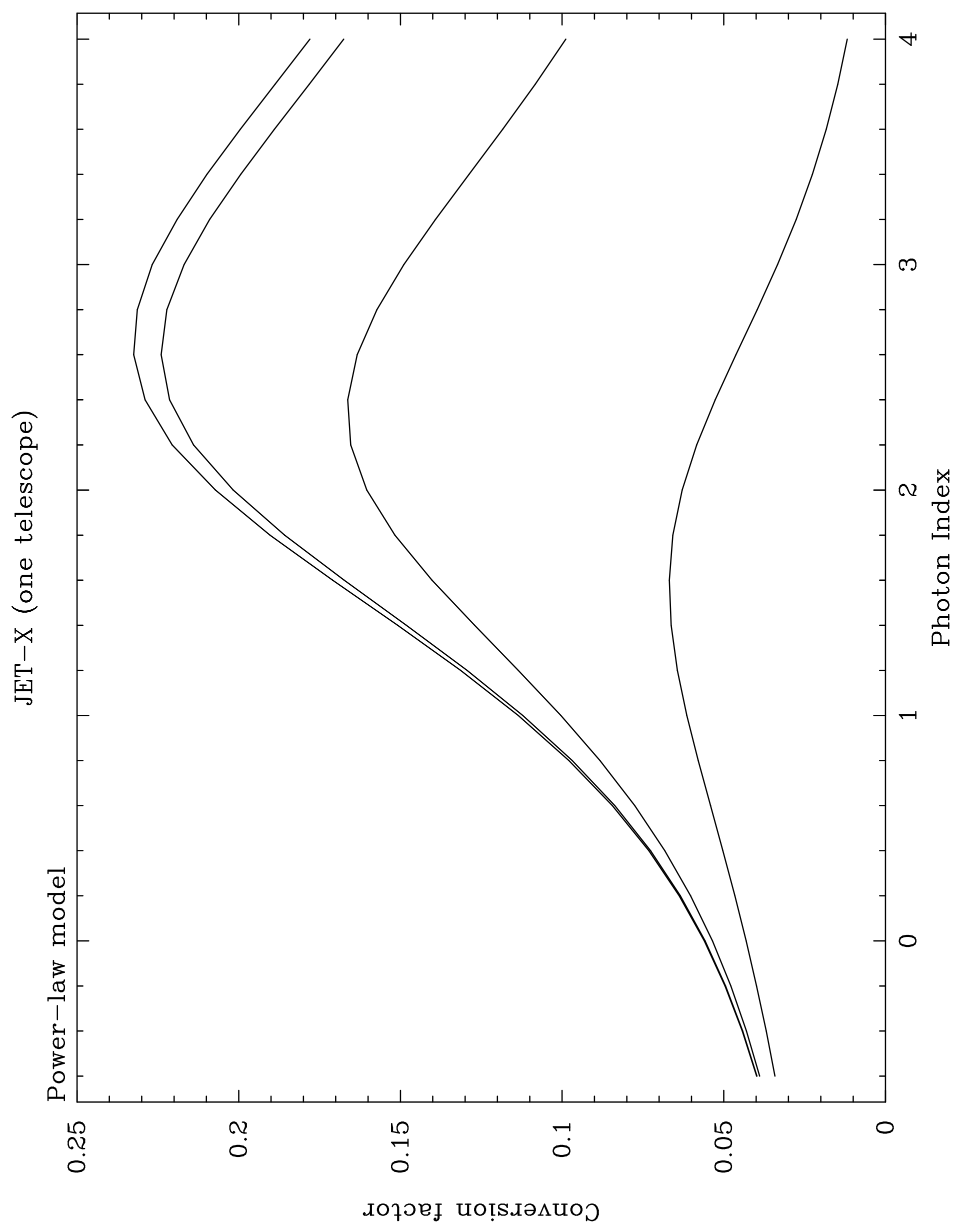

Figure 14: Energy Conversion Factor versus power-law photon indexes for different interstellar absorptions: 10^{19}, 10^{20}, 10^{21} and 10^{22} cm^{-2} starting from the top.

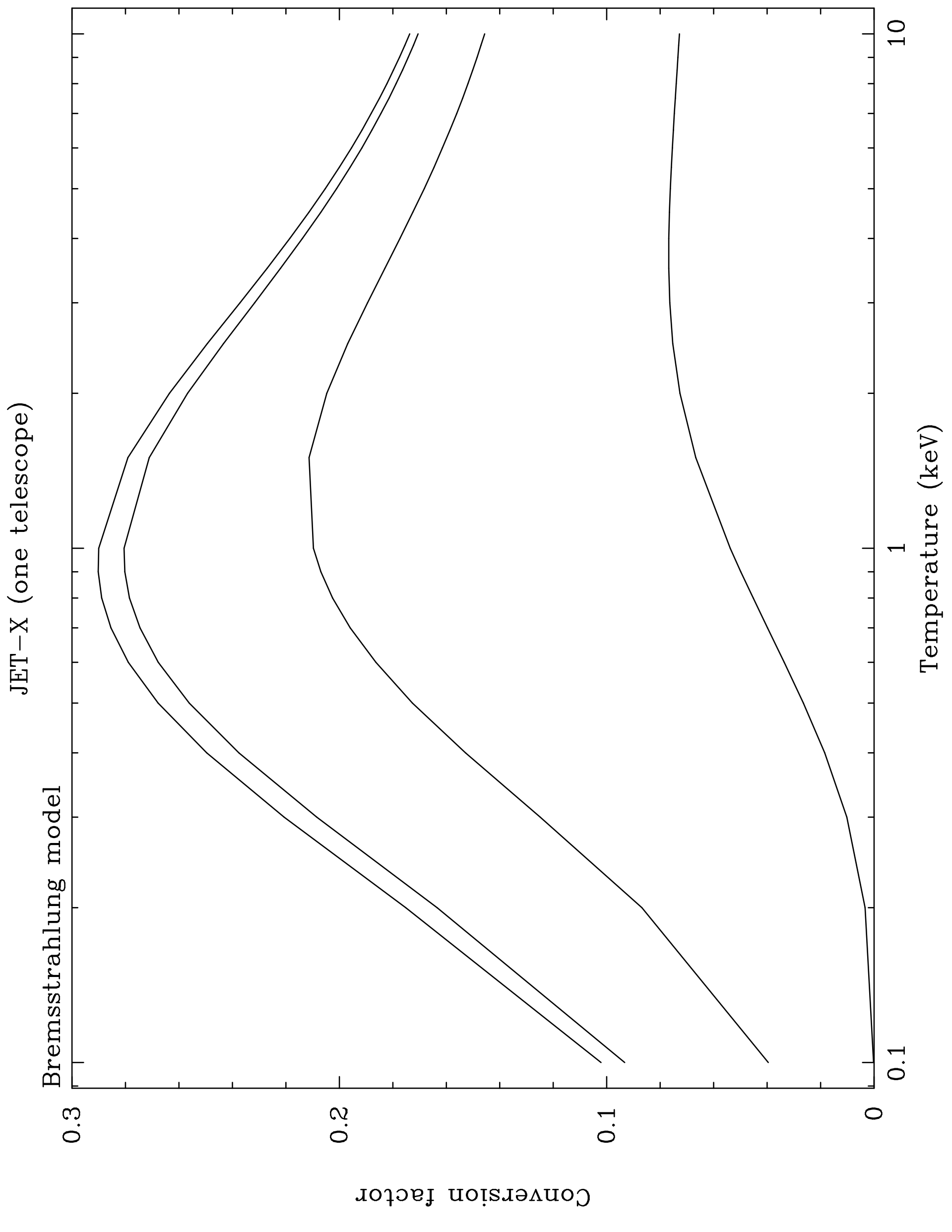

Figure 15: Energy Conversion Factor versus bremsstrahlung temperature (in keV) for different interstellar absorptions: 10^{19}, 10^{20}, 10^{21} and 10^{22} cm^{-2} starting from the top.

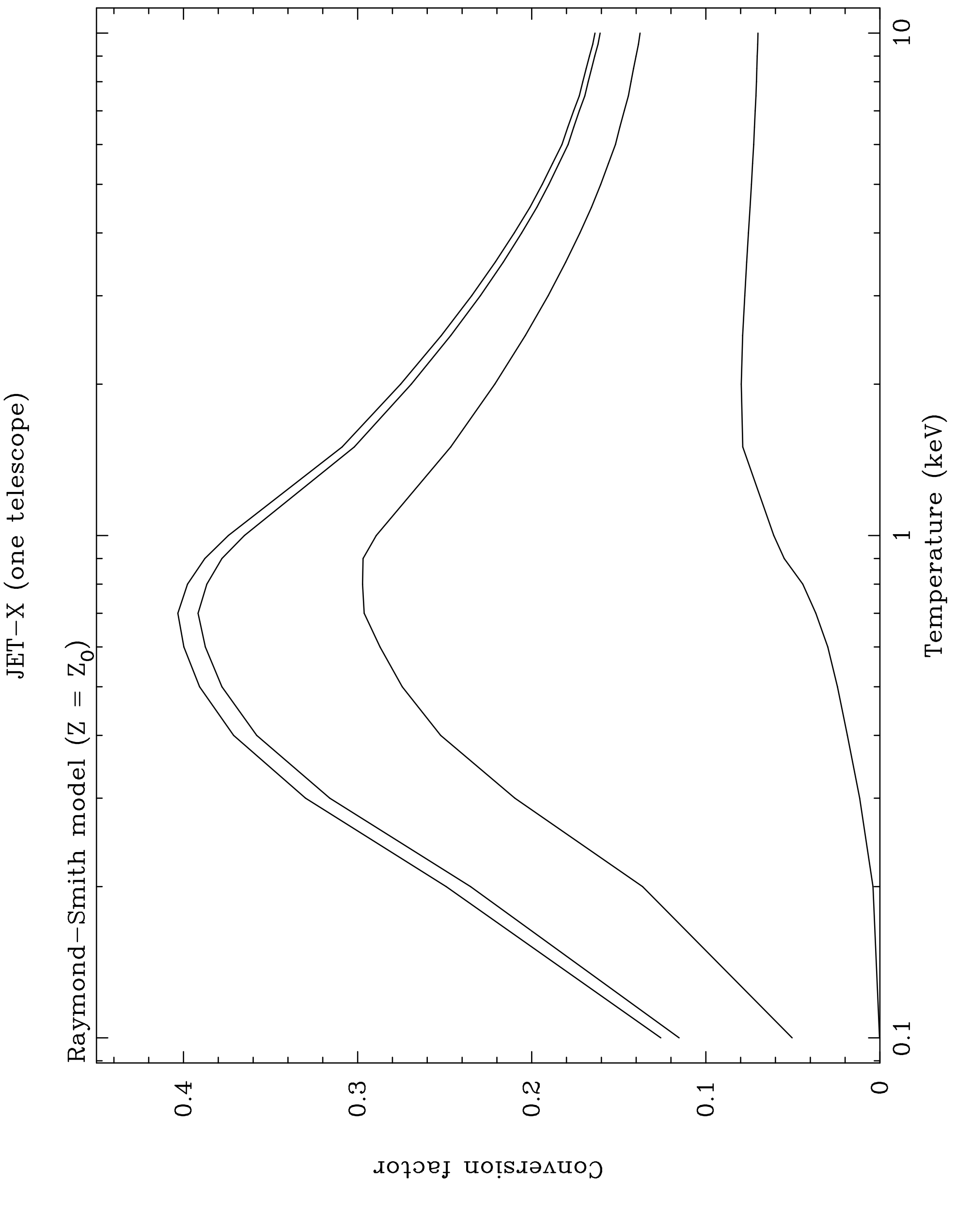

Figure 16: Energy Conversion Factor versus Raymond-Smith temperature (in keV) assuming a solar metallicity and for different interstellar absorptions: 10^{19}, 10^{20}, 10^{21} and 10^{22} cm^{-2} starting from the top.

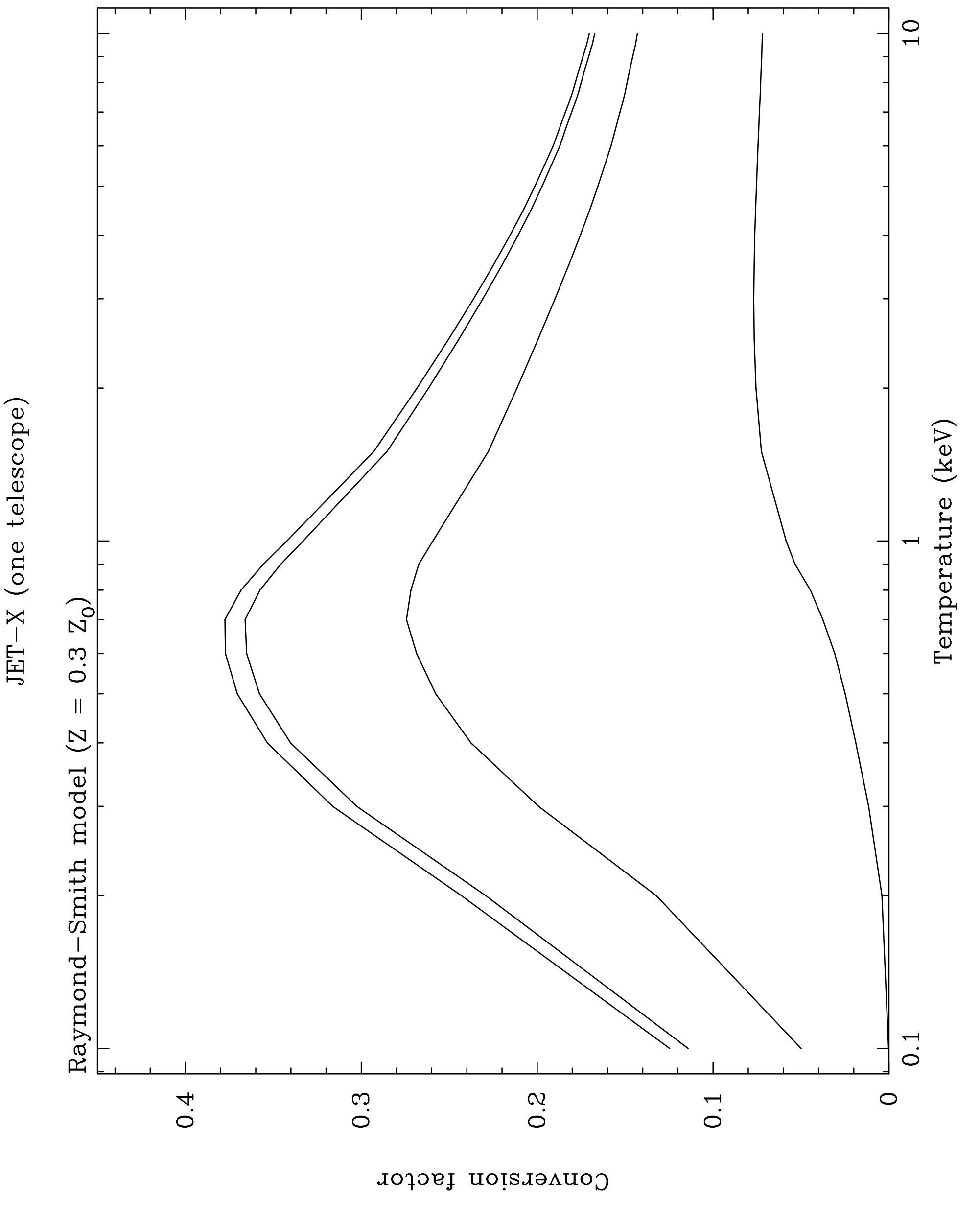

Figure 17: Energy Conversion Factor versus Raymond-Smith temperature (in keV) assuming a metallicity equal to 0.3 the solar value and for different interstellar absorptions: 10^{19}, 10^{20}, 10^{21} and 10^{22} cm^{-2} starting from the top.

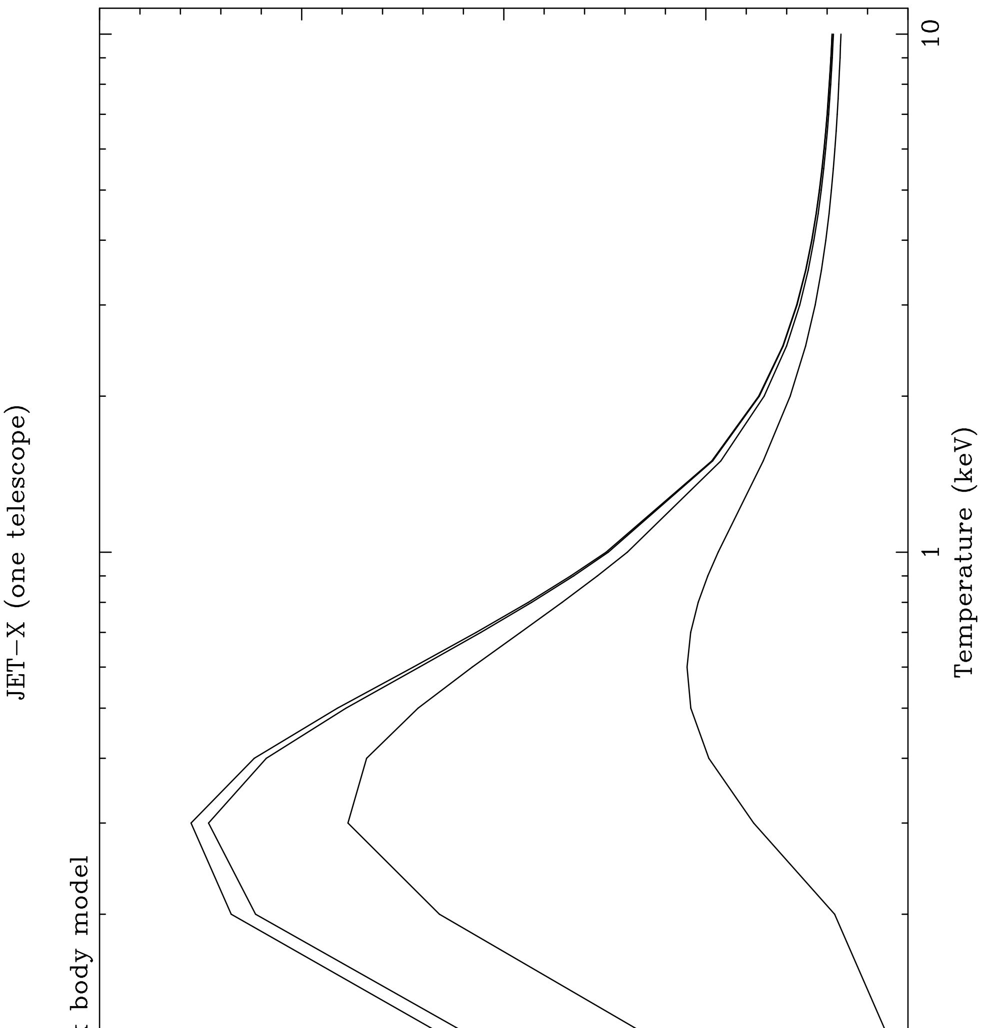

Figure 18: Energy Conversion Factor versus black body temperature (in keV) for different interstellar absorptions: 10^{19}, 10^{20}, 10^{21} and 10^{22} cm^{-2} starting from the top.

8 Proposal Preparation and Submission. TBD

TBD